Advances in magnetometry

2007 J. Phys.: Condens. Matter 19 165217

(http://iopscience.iop.org/0953-8984/19/16/165217)

IOP PUBLISHING JOURNAL OF PHYSICS: CONDENSED MATTER

J. Phys.: Condens. Matter **19** (2007) 165217 (28pp) doi:10.1088/0953-8984/19/16/165217

Advances in magnetometry

Alan Edelstein

US Army Research Laboratory, Adelphi, MD 20783, USA

Received 22 September 2006, in final form 18 January 2007
Published 6 April 2007
Online at stacks.iop.org/JPhysCM/19/165217

Abstract

This article describes many of the advances in magnetometry. Because much of the recent progress in magnetometry is built on current technology, and to put these advances in the proper perspective, a general discussion of magnetometry will also be presented. The progress includes a remarkable increase in the magnetoresistance of some devices, improved signal processing, and some new types of magnetometer. The large increase in magnetoresistance is a result of an increased understanding of quantum mechanical spin dominated transport in restricted geometries such as multilayers and magnetic tunnel junctions. The new types of magnetometer include magnetoelectric sensors, extraordinary magnetoresistance sensors, and sensors that incorporate MEMS technology. These advances in magnetometer technology offer orders of magnitude increases in sensitivity and/or large decreases in cost and power consumption. Major technological limitations of current magnetic sensors are also discussed.

(Some figures in this article are in colour only in the electronic version)

1. Introduction to magnetometry

In this paper some aspects of magnetic sensors will be reviewed, but the emphasis will be on advances in magnetometry. These advances include zigzag anisotropic magnetometers [1], magnetic tunneling junction sensors with MgO barriers [2, 3], magnetoelectric sensors [4, 5], microelectromechanical system (MEMS)-based sensors [6], and chip-scale atomic magnetometers [7]. In addition, two topics of less technological interest, namely the magnetoresistance of C_{60} molecules with ferromagnetic electrodes [8] and the quantized conductance [9] in break junctions, will be covered because of their scientific interest.

The motivation for this research in magnetic sensors is their many applications. The applications of magnetic sensors include measuring currents, compassing, correcting for the drifts of gyroscopes, detecting unexploded ordnance, space exploration, and measuring the magnetic fields generated by the brain. Magnetic sensors have assisted mankind in analyzing and controlling thousands of functions for many decades. Read heads in computers have magnetic sensors. Automobiles use magnetic sensors to determine the position in several places

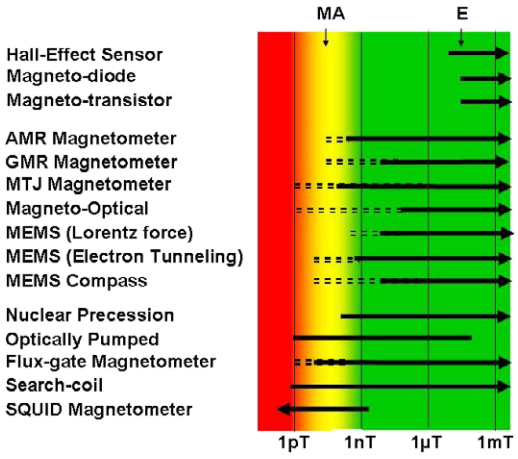

Figure 1. Estimate of sensitivity of different magnetic sensors. The symbols E and GMN are used to indicate the strength of the earth's magnetic field and geomagnetic noise, respectively.

such as the engine crank shaft and wheel braking. Factories have higher productivity because of the precise stability and low cost of magnetic sensors. Aeroplanes fly with higher safety standards because of the high reliability of non-contact switching with magnetic sensors. The large commercial applications that have driven the technology are the need for improved read heads and the potential applications of magnetic random access memory (MRAM) [10]. Here the focus will be on low frequency applications. The major applications of magnetic sensors can be placed into the following four categories: measuring fields stronger than the earth's field, measuring perturbations in the earth's field, measuring small changes or gradients in generated or induced magnetic fields, and medical/biological applications. Magnetic sensors provide a very rugged, reliable, and maintenance-free technology. The subject has been reviewed previously [11–14].

Most of the more common magnetic sensor technologies are listed in figure 1, which compares approximate sensitivity ranges. In the figure, the symbols E and GMN are used to indicate the strength of the earth's magnetic field and geomagnetic noise, respectively. Because of the large magnitude of the earth's magnetic field, sensitive sensors must either have a large dynamic range or use some means to decrease the field at the position of the sensor. Geomagnetic noise has a $1/f$-like frequency spectrum and is spatially correlated over distances of the order of kilometres because it is arises from sources that are spatially large such as currents in the ionosphere that are driven by tidal forces and winds [15]. Thus, by taking the difference between the readings of two or more spatially separated sensors it is possible to measure magnetic field changes smaller than the geomagnetic noise. There are many factors other than sensitivity such as cost, frequency response, size, and power requirements, that determine which sensor is best suited for an application. With regard to frequency response it is important to note that for frequencies above 10 Hz, coil-based magnetometers using the Faraday effect can have sensitivities of order 100 fT.

There are two basic kinds of magnetic sensor: vector magnetometers that measure the components of the magnetic field and total field magnetometers (also called scalar magnetometers) that measure the magnitude of the magnetic field. One might think that since vector magnetometers provide additional information, vector magnetometers are always better than magnetometers that measure only the magnitude of the field. For some applications, however, scalar magnetometers are much better than vector magnetometers. Consider using a magnetometer on a moving vehicle and trying to detect small changes due to the presence of ferromagnetic objects. Rotational vibrations due to the vehicle's motion will generate changes

in the vector components of the earth's field detected by a vector magnetometer that are difficult to separate from the signal. These changes are given by

$$\mathrm{d}B/\mathrm{d}t = B \cdot \sin\theta \cdot \mathrm{d}\theta/\mathrm{d}t \tag{1}$$

where B is the magnitude of the magnetic field, θ is the angle between the magnetic field and the measuring direction of the vector sensor, and t is the time. If for example $B = 50\,000$ nT, $\theta = 45°$, and $\mathrm{d}\theta/\mathrm{d}t = 0.1°\ \mathrm{s}^{-1}$, then $\mathrm{d}B/\mathrm{d}t = 61.7\ \mathrm{nT\,s}^{-1}$. Such a change is often much bigger than the change due to the presence of a ferromagnetic object. Accurately computing the total field from the vector components is difficult because the sensitivities of the three vector magnetometers must be identical and their axes exactly perpendicular. Thus, in this application a total field magnetometer is much better than a vector field magnetometer.

The following sections discuss vector magnetometers and scalar magnetometers. Next there is a section on some of the factors that limit magnetometry followed by the conclusion. The units for magnetic field in air are: 1 T = 10^4 Oe = 10^4 G = 10^9 nT = 10^9 gamma = 10^{12} pT = 10^{15} fT = $1/4\pi \times 10^7$ ampere-turns/metre. Note that we are not distinguishing here between H and B.

2. Vector magnetometers

Vector magnetometers suffer from noise [16], especially $1/f$ noise [17]. One attempt at mitigating the effect of $1/f$ noise is the work done on a device, the MEMS flux concentrator [6, 18], which shifts the operating frequency above the range where $1/f$ noise dominates. The device is discussed further in section 2.10.

2.1. Search-coil magnetometer

A voltage will appear between the leads in a search-coil magnetometer that is proportional to the rate of change of the flux through the coil. The flux through the coil will change if the coil is in a magnetic field that varies with time, if the coil is rotated in a uniform field, or if the coil is moved through a non-uniform field. Usually a rod of a ferromagnetic material with a high magnetic permeability is inserted inside the coil to increase the flux density. The frequency response of the sensor may be limited by the ratio of the coil's inductance to its resistance, which determines the time it takes the induced current to dissipate when the external magnetic field is removed. Their useful frequency range is typically from 1 Hz to 1 MHz, the upper limit being that set by the ratio of the coil's inductance to its resistance.

2.2. Fluxgate magnetometer

Fluxgate magnetometers [19] are widely used sensors to make sensitive, low frequency measurements. The fluxgate magnetometer consists of a ferromagnetic material wound with two coils, a drive and a sense coil. It exploits magnetic induction together with the fact that all ferromagnetic materials saturate at high fields. When a sufficiently large sinusoidal current is applied to the drive coil, the core reaches its saturation magnetization once each half-cycle. As the core is driven into saturation, the reluctance of the core to the external magnetic field being measured increases, thus making it less attractive for any additional magnetic field to pass through the core. This change is detected by the sense coil. The voltage output from the sense coil consists of even-numbered harmonics of the excitation frequency. For readout, the second harmonic which is proportional to the external magnetic field is extracted and rectified. For maximum sensitivity, the magnetic field–magnetic induction (B–H) curve of the core should

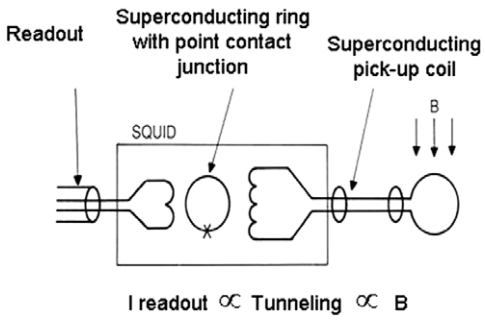

Figure 2. Schematic diagram of a superconducting quantum interference device (SQUID).

be square, because this produces the highest induced electromotive force (emf) for a given value of the magnetic field. For minimum power consumption, the core material should have low coercivity and saturation values. The sensitivity range is from 10^{-2} to 10^{7} nT. The upper limit on the frequency range, about 10 kHz, is limited by the ferromagnetic core material. Fluxgate magnetometers consume more power than search coil magnetometers because of the need to saturate or at least partially saturate the core material. Unlike search coil magnetometers, fluxgate magnetometers can measure low frequency fields. Some fluxgate magnetometers reduce power consumption by operating the sensor on a minor hysteresis loop, thus not driving the core from saturation to saturation. These minor-loop fluxgate magnetometers are much more sensitive to the drive and readout electronics than the major-loop versions, whose performance is governed mostly by the core material's properties.

2.3. Superconductor magnetometers

2.3.1. SQUID sensors. The most sensitive of all instruments for measuring a magnetic field at low frequencies (<1 Hz) is the superconducting quantum interference device (SQUID) [20, 21], illustrated in figure 2. The flux through the ring is quantized [22, 23] and the flux can only take on values that are integer multiples of a basic quantum of magnetic flux $\phi_o = ch/2e \approx 2 \times 10^{-7}$ gauss cm^2. In a SQUID, the periodic flux variations are exploited to measure the current in the superconductor. Typically, the ring is inductively coupled to a radio-frequency circuit that both supplies a known bias field and serves as the detector output. Changes in the field can be measured by counting the peaks that are a result of the flux quantization, or a feedback loop can be employed to lock the radio-frequency circuit onto a single peak. The feedback current is then a measure of the ambient field. One can also form a dc SQUID by employing two Josephson junctions in the ring. When the two weak links are matched properly through design, the current in the ring has a dc response to the flux going through it.

The superconducting ring in a SQUID contains a weak link, a narrow constriction in the superconductor, or a point–contact junction. Sensitivity is improved by coupling the ring to a larger superconducting loop that gathers flux over an area of several square centimetres. Using superconducting properties, one can form a dc transformer between the sense loop and the SQUID readout. The device has three superconducting components: the SQUID ring itself, the radio-frequency coil, and the large antenna loop. The sensitivity of SQUIDs is limited by the magnetic field noise and for commercial dc SQUIDs this noise [24] is of order 10 fT. The ability to set a null level by adjusting the bias field in the radio-frequency circuit makes the device particularly useful for differential field measurements. For example, if the null level is set to the average terrestrial magnetic field, the instrument will readily detect anomalies in the field. The sensing loop can be configured to be sensitive to field gradients. To date, magnetometers [20]

built with high superconducting transition temperature materials (HTSCs) [25, 26] do not have as good a sensitivity as those built with low temperature superconductors. The high sensitivity of SQUIDs allows them to be used in astronomy [27] and in geological [28] and medical applications [29]. SQUIDs also provide one of the more promising approaches to quantum computing [30, 31]. A digital SQUID sensor based on a single-flux quantum with a large slew rate has been developed [32].

2.3.2. Using the Meissner effect. The exclusion of magnetic fields by induced currents in superconductors below a critical field, the Meissner effect [33], has been used [34] in a superconducting flux-to-field transformer to construct a magnetometer. The magnetometer has a superconducting loop perpendicular to the field direction with a width that is 0.7 times the radius and a micron size constriction. The shielding current, which is greatly enhanced in the constriction, generates a field that is measured by a low-noise giant magnetoresistance (GMR) sensor located near the constriction. The small size prototype can be used at 77 K and is capable of measuring 32 fT at 4 K.

2.4. Hall effect sensor

The Hall effect sensor [35] is a low cost sensor that can operate over a wide temperature range. Semiconductors must be used because the Hall effect is very small in metallic conductors. Since there are fewer conduction electrons in a semiconductor, if the total current through it is the same as that through a metal, the electrons in the semiconductor must have a much higher drift velocity than those in the metal. Because of the electron higher velocity in semiconductors, the electrons experience a stronger force and the Hall voltage is increased. Inexpensive Hall effect sensors are generally made of silicon. More sensitive sensors are made of the III–V semiconductors because they have higher electron mobilities than silicon. The silicon devices have a sensitivity range of 10–1000 G. The indium antimonide sensors extend the lower limit to 10^{-3} G. The upper frequency limit of Hall effect sensors is about 1 MHz.

2.5. Magnetoresistive magnetometers

Magnetoresistance magnetometers [36] utilize a change in resistance ΔR, caused by an external magnetic field H. Values for the magnetoresistance MR are given as $\Delta R/R$ where R is the $H = 0$ value of the resistance. The types of magnetoresistance sensors that will be discussed in this section include anisotropic magnetoresistance (AMR), giant magnetoresistance (GMR), magnetic tunnel junction (MTJ), and extraordinary magnetoresistance sensors. Magnetoresistance magnetometers represent the class of magnetic sensor that has shown the greatest recent improvement. Figure 3 illustrates this progress for several kinds of magnetoresistance sensors. The largest room-temperature values of the MR for fields $H \leqslant 10$ Oe are plotted. Larger values of MR have been obtained at lower temperatures and/or at higher fields, but these values are of less interest for magnetometry. Because of this progress, we shall discuss magnetoresistance sensors in some detail. Magnetoresistance magnetometers are very attractive for low cost applications because they are simply energized by applying a constant current and the output voltage is a direct measure of the magnetic field. Mapps has written a review [37] of magnetoresistance sensors that includes a discussion of the effect of Barkhausen noise. The values of MR for magnetometry are usually expressed as the percentage change in the resistance per Oe or in the voltage change out per volts in per change in field. Optimally a bridge circuit and other methods are used to minimize the dc offset and the effect of thermal drift. Modulation techniques such as that of the MEMS flux concentrator [18] are

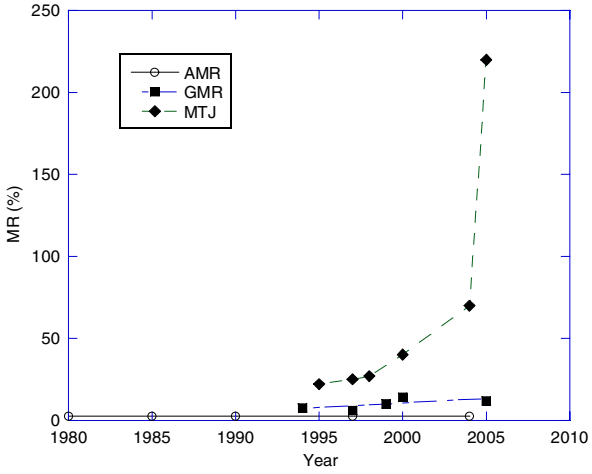

Figure 3. Progress in magnetoresistance sensors as shown by the increase in the room-temperature magnetoresistance of magnetic sensors for fields less than about 10 Oe.

useful for eliminating the dc offset. At low frequencies, sensors with less $1/f$ noise may be preferred over sensors with larger values of *MR*. Stutzke *et al* [38] made low frequency noise measurements on several commercial magnetoresistance sensors. They found that for AMR and GMR sensors both electronic and magnetic effects contribute to the noise and the maximum noise occurs at the bias field that maximizes the sensitivity. They also found that the noise in MTJ sensors is primarily due to resistance fluctuations in the tunnel barrier and is independent of the bias field. They found that the best low-field detectivity of commercial *MR* sensors was 100 pTHz$^{-1/2}$ at 1 Hz. Jiang *et al* [39] studied the noise in MTJ sensors and found that the power spectrum was $1/f$-like at low frequencies. At high frequencies, the noise becomes frequency independent and is due to Johnson–Nyquist and shot noise. Their findings for the MTJ sensors they studied were different from those of Stutzke *et al* in that the noise power in the hysteresis loops is strongly field dependent. Some of the noise is magnetic in origin because the noise increases when the magnetic field causes the magnetization of either the pinned or free layer to undergo a reversal.

2.5.1. Anisotropic magnetoresistance (AMR) sensors. AMR sensors use materials, such as permalloy (an alloy containing about 80% nickel and 20% iron), whose resistance depends on the angle between the magnetization and the direction of current flow [40]. For example, the resistance of permalloy decreases as the direction of magnetization rotates away from the direction in which the current flows and is lowest when the magnetization is perpendicular to the direction of current flow. The resistance changes roughly as the square of the cosine of the angle between the magnetization and the direction of current flow. Figure 4(a) illustrates the resistance as a function of the angle between the magnetization and direction of the current. To have a linear response at low fields, it is desirable to have the current flowing at a 45° angle with respect to the magnetization. This is typically accomplished using shorting straps in the so-called 'barber pole' arrangement. In the 'barber pole' arrangement there are shorting strips that cause the current direction to be at 45° with respect to the direction of the magnetization. The need for using the barber pole geometry can be eliminated by using a zigzag-shaped geometry of thin-film elements [1] as shown in figure 5. This geometry forces the direction of the magnetization to alternate as confirmed by scanning electron microscopy with polarization analysis (SEMPA) measurements. These zigzag sensors have a sensitivity of 3.54 mV/(V kAm^{-1}) in the parallel field configuration.

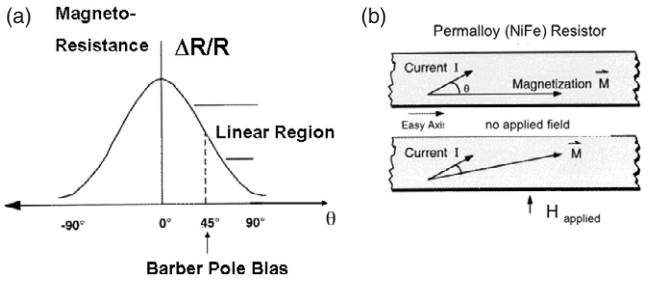

Figure 4. Anisotropic magnetoresistance (AMR) sensor: (a) resistance versus angle θ between the magnetization and the direction of current flow, (b) change in θ due to the application of a magnetic field.

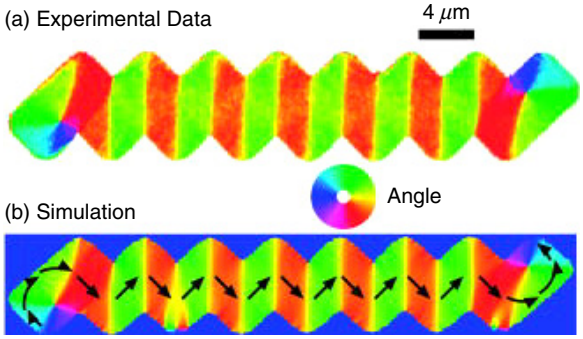

Figure 5. (a) Experimental SEMPA image of the zigzag structure. (b) Simulation performed on the same geometry using the object oriented micromagnetic framework (OOMMF). OOMMF is a public domain program. The magnetization direction maps onto the angle colour map ring. Taken from [1].

Permalloy is the most common material for AMR sensors because it has a relatively large magnetoresistance and because its characteristics are compatible with the fabrication techniques employed to make silicon integrated circuits. The magnetoresistance [41] of permalloy is less than 4%. As shown in figure 6(a), an integrated sensor normally consists of four permalloy resistors sputter-deposited on a silicon substrate to form a bridge. An offset voltage in a magnetoresistive bridge can arise from the inherent resistance of the four resistors that are not precisely matched. In designing anisotropic magnetoresistance bridges, one can use a method that greatly reduces the offset from mismatches in the four resistors. This set/reset method is illustrated in figure 6(b). By changing the direction of the magnetization in the thin film, the bridge output changes sign. Figure 6(b) shows the bridge voltage produced from an applied field when the magnetization is set in one direction and then reversed (reset). This setting of the magnetization is done by applying a strong magnetic field for a short time along the direction desired. By subtracting the voltage reading when the sensor is in the reset mode from the voltage reading in the set mode, the inherent resistance and its noise (such as temperature effects) is cancelled and the resulting value represents twice the output for the applied field measurement. Typical AMR sensors have a sensitivity range of 10^3 to 5×10^6 nT with open-loop readout electronics. With closed-loop feedback readout electronic methods, the minimum detectable field can be reduced to better than 0.1 nT for limited bandwidths.

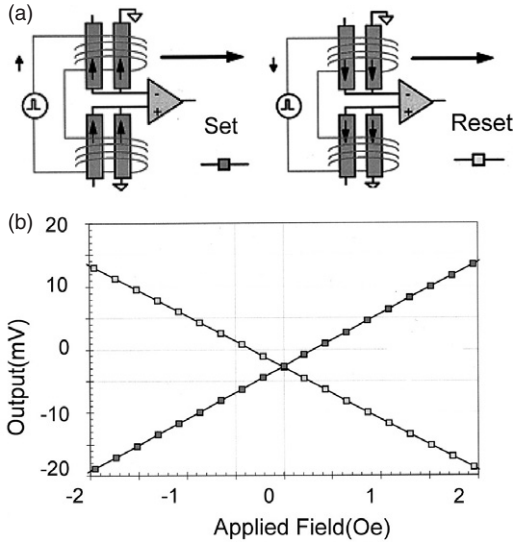

Figure 6. Figure illustrating set and reset operation of an anisotropic magnetoresistance sensor: (a) direction of current flow in coils that set and reset the direction of the magnetization of the cores, (b) output voltage as a function of the field when the coil operates in the set and reset mode.

2.5.2. Giant magnetoresistance (GMR) sensors. Larger changes in magnetoresistance were observed [42, 43] in planar structures of metals. The effect was named giant magnetoresistance or GMR. In its simplest form, called a spin valve [44], GMR is achieved by using a four layer structure that consists of two thin ferromagnets separated by a conductor. The fourth layer is an antiferromagnet that is used to pin (inhibit the rotation) the magnetization of one the ferromagnetic layers. The ferromagnet layer that is being pinned is between the conductor and the antiferromagnet. The pinned ferromagnet is called the hard ferromagnet and the unpinned ferromagnet is called the soft ferromagnet. Electrons can travel more easily either parallel to the layers or perpendicular to the layers if the magnetizations of the two ferromagnets are parallel to one another. The reason for this is that when the magnetizations are parallel, electrons suffer less scattering in going from an electronic band structure state in one of the ferromagnets into a similar or identical electronic band structure state in the other ferromagnet [42, 43, 45, 46]. The difference in resistivity between the case when the magnetizations are parallel and when they are antiparallel can be as large as 12.8% at room temperature [47]. To optimize the effect, the layers must be very thin, about a nanometre thick. For the response of the sensor to be a linear function of the field, it is necessary that the soft ferromagnet have its easy axis of magnetization in zero field perpendicular to the magnetization of the pinned ferromagnet. The zero field orientation of the two magnetizations is depicted in figure 7(a). The resistance is measured either in the plane of the ferromagnetic layers or perpendicular to this plane. It is possible to eliminate the antiferromagnetic pinning layer by adjusting the thickness of the nonferromagnetic conducting layer so that the two ferromagnets are coupled antiferromagnetically [48]. In this case, the resistance is maximum at $H = 0$. A difficulty with this approach is that the sensor is insensitive and nonlinear near $H = 0$.

The basic three or four layer structure can be repeated to create a multilayer geometry. This multilayer geometry increases the percentage resistance change because it increases the probability of spin flip scattering by increasing the number of interfaces where spin flip scattering occurs. It is very desirable that the layers should be very smooth to minimize coupling between the layers [49]. GMR sensors can be used in two different geometries, the current in the plane geometry (CIP) and the current perpendicular to the plane geometry (CPP). GMR sensors have been used in computer read heads, but several and possibly all of

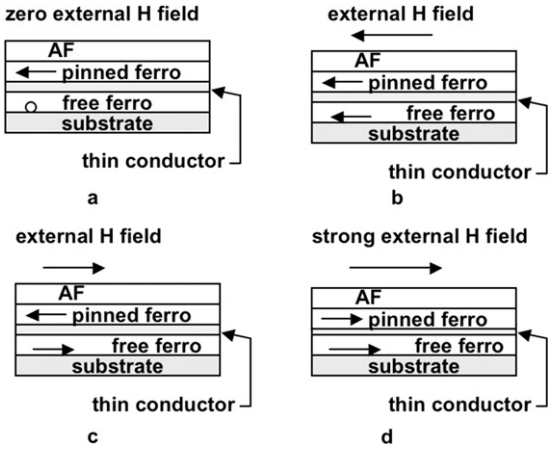

Figure 7. Orientation of the magnetization of the ferromagnetic layers in a GMR spin valve for different external fields H. (a) $H = 0$, the magnetization of the free ferromagnetic layer is perpendicular to the magnetization of pinned ferromagnet, $R = R(0)$. (b) Low resistant state, H parallel to the magnetization of the pinned ferromagnet, $R < R(0)$. (c) High resistant state, H directed opposite to the magnetization of the pinned ferromagnet, $R > R(0)$. (d) H large enough to unpin the pinned ferromagnet, $R < R(0)$.

the largest manufacturers are currently using magnetic tunnel junctions (see the next section) in their read heads. However, manufacturers are considering using CPP GMR sensors in the future to minimize the resistance–area (RA) product. How the directions of the magnetization of the two ferromagnetic layers change with the application of a magnetic field is illustrated in figure 7. One does not have to use any set/reset feature with spin valves, but they tend to have more $1/f$ noise than AMR sensors. Present GMR sensors can be used in fields as small as 10 nT at 1 Hz to as large as about 10^8 nT.

CPP sensors are usually multilayer devices. Because the length of the resistor is equal to the thickness of the stack, the resistance will be very low unless the area is reduced by microfabrication techniques. These techniques are discussed by Martin *et al* [50]. The *MR* in CPP Fe/Cr multilayers was 108% at 4.2 K [51], but the *MR* is reduced to 12% at room temperature. For the same structure, the *MR* is larger by as much as a factor of 10 for the CPP geometry than for the CIP geometry. The important length scale for CPP-GMR is the spin-flip diffusion length. This material dependent length typically varies between 5 and 100 nm.

2.5.3. Magnetic tunnel junction sensors. Magnetic tunnel junctions (MTJ) or spin dependent tunneling (SDT) sensors [52, 53], first fabricated in 1995, have a structure similar to the four layer structure described above in GMR sensors. Again there are two ferromagnets separated by an intervening layer and the magnetoresistance is a function of orientation of the two ferromagnets, but in this case the intervening layer is an insulator. In MTJ sensors, the conduction occurs by tunneling of electrons through the insulator. Based on a spin-polarized tunneling model [54] the magnetoresistance ratio *MR* or $\Delta R/R$ is given by

$$\Delta R/R = (R_a - R_p)/R_p = 2P_1P_2(1 - P_1P_2) \tag{2}$$

where R_p and R_a are the resistances when the two ferromagnets are parallel and antiferromagnetic, respectively, and P_1 and P_2 are the spin polarizations of the two ferromagnets at the Fermi surface. The spin polarizations in the two ferromagnets are determined by the spin dependence of the density of states near the Fermi energy. The

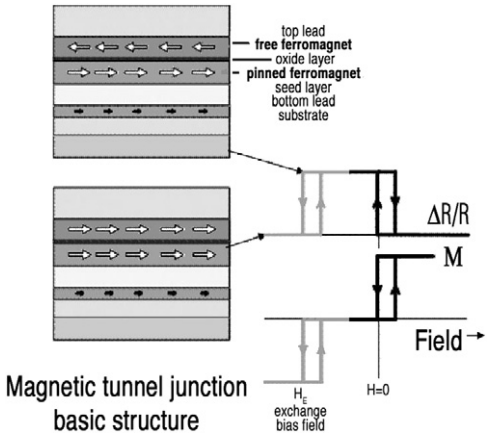

Figure 8. Magnetic tunnel junction (MTJ) sensor. In the application shown the device is a switch. A different design must be employed if the device is to be used as a linear sensor.

MR is also a function of the tunneling matrix elements. Because of the strong dependence of polarization, it is expected that one could get very large *MR* values in half-metallic ferromagnets, such as the manganite perovskites and CrO_2. Large values of about 1000% were observed [55] for the *MR* of manganite perovskites at 14 K, but only a very small effect was observed at room temperature. Currently, there is not a half-metallic ferromagnet with a high Curie temperature that can be used in room-temperature MTJ sensors. Even if there were one, to make an MTJ it would be necessary that the material remain a half-metallic ferromagnet near the barrier interface. Figure 8 shows the structure of an MTJ sensor and how the magnetization and resistance change as a function of magnetic field. The device shown is for a read head in a magnetic hard drive. For a sensor used to determine an arbitrary field, the change in resistance should be linear in field and the hysteresis should be zero.

There are technical issues in preparing tunnel junctions. Because the wave function amplitude decreases exponentially in the barrier, the barrier must be thin, about 1 nm thick. One must avoid shorting the junctions either in fabricating the junction or by accidentally applying an electric field across the junction large enough that it creates a pin hole or metallic bridge in the barrier. The layers also should be very smooth to minimize Néel coupling between the layers [49]. As was discussed above for spin valves, the magnetization of one of the ferromagnetic layers is pinned by being in contact with a layer of an antiferromagnet. For the response of MTJ sensors to be a linear function of the field it is necessary that the soft ferromagnet have its easy axis of magnetization in zero field perpendicular to the magnetization of the pinned ferromagnet. Making the magnetization of the soft ferromagnet perpendicular to the magnetization of the hard ferromagnet can be accomplished by applying a magnetic field [56] or using shape anisotropy. Using a field usually greatly increases the power consumption. Instead, Lacour *et al* [57] obtained the required perpendicular configuration by growing the 'soft' electrode on a vicinal step-bunched Si(111) substrate tilted by 4° towards the $[11\bar{2}]$ direction. This generates a uniaxial anisotropy along the larger axis of the steps [58]. In at least one case, it was found that chemical reactions between the electrodes and the barrier can lead to large decreases in the barrier resistance [59]. Because of these difficulties, the choice of barrier is often based on finding a material that permits the successful fabrication of tunnel junctions. For example, amorphous or microcrystalline aluminium oxide was often used as the tunneling barrier in MTJ sensors because one could obtain thin, smooth, pinhole-free layers with controllable thicknesses. These barriers could be produced by depositing 1–2 nm of Al and then oxidizing the Al in oxygen by using a glow discharge or by letting a natural oxide

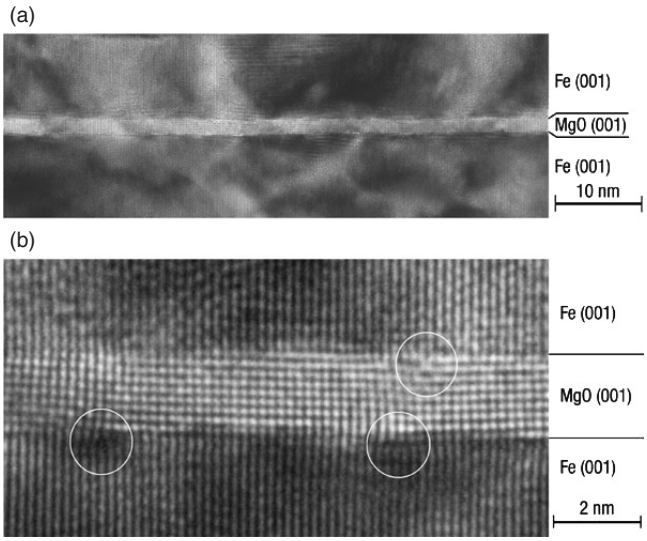

Figure 9. (a) TEM image of the Fe(100)/Mg((100)/Fe(100) MTJ. (b) Enlarged TEM of (a); lattice dislocations are circled. Taken from [3].

form when the Al is exposed to oxygen. In January 2004, *MR* values as large as 70% at room temperature were reported [60] for MTJ sensors with amorphous aluminium oxide barriers. Aluminium oxide seemed to be the best barrier material.

This situation was totally changed by theoretical calculations [61, 62] that showed that the tunneling conductance is strongly dependent on the symmetry of the electron states of the electrodes and the evanescent electron states in the barrier. Butler *et al* [61] performed first principles calculations of the *MR* of epitaxial Fe(100)/MgO(100)/Fe(100) sandwiches. They found that Bloch states with different symmetry have different decay rates in the barrier. Butler *et al* made the prediction that the magnetoresistance would increase with barrier thickness. This followed from the different character of the states at the Fermi energy in majority and minority channels for tunneling. In the majority channel, the state with Δ_1 symmetry is able to couple states into the MgO barrier. In the minority channel, interface resonance plays a more important role. Thus, they find that the conductance of the minority channel will decrease faster with increasing film thickness than the majority channel. However, their calculations of the conductance associated with the interfacial resonance states are dependent on the nature of the interface. Unfortunately, experimental structure information about interfaces is often lacking. In contrast to Butler *et al*, Mathon *et al* [62] predicted that the *MR* is only weakly dependent on the thickness of the MgO barrier.

Later two groups reported [2, 3] *MR* values of 180–220% for MTJ sensors with MgO barriers at room temperature. Yuasa *et al* [3] started with a single crystal of MgO(001) and used molecular beam epitaxy (MBE) techniques to produce a single crystal Fe/MgO/Fe MTJ. The MgO(001) was grown epitaxially at room temperature using an electron beam source. Transmission electron microscopy (TEM) images showing the single crystal lattices of the MTJ are shown in figure 9. The *MR* obtained by Yuasa *et al* at 20 and 293 K as a function of MgO thickness t_{MgO} is shown figure 10. Several things should be noted in this figure other than the large values of *MR*. First, the *MR* is not extremely temperature dependent. Second, as predicted by Butler *et al*, the values of *MR* increase as a function of t_{MgO}. Third, the values of *MR* are an oscillating function of t_{MgO} with a period of 0.30 nm. They attributed this last result as an indication that the wavefunction maintained its coherency across the barrier.

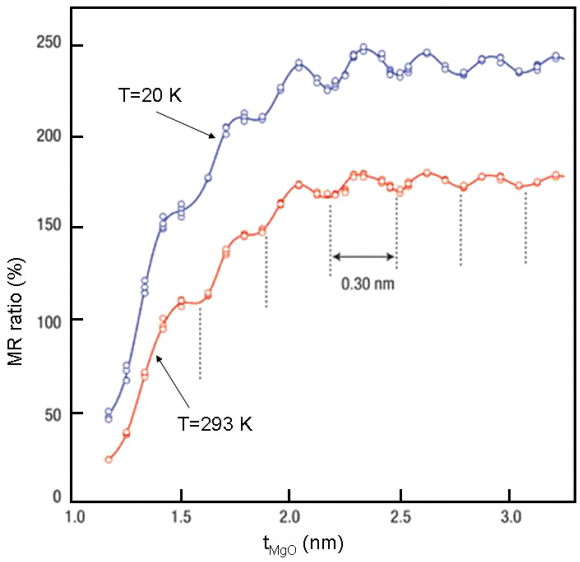

Figure 10. *MR* in an MTJ as a function of the thickness of the MgO tunneling barrier. Taken from [3].

After annealing their MTJ devices with MgO oxide barriers, Parkin *et al* [2] obtained room-temperature *MR* values of about 220%. These values are even larger than the room-temperature *MR* values shown in figure 10. In contrast to Yuasa *et al* who used single crystalline samples, Parkin *et al* used a combination of magnetron and ion beam sputtering to produce polycrystalline layers that had a (001) texture. The substrate was Si(100) covered with an amorphous layer of SiO_2. They produced devices with good thermal stability that could be integrated with CMOS circuits for MRAM applications. An antiferromagnetic layer of $Ir_{22}Mn_{78}$ was used to exchange bias the lower ferromagnetic layer. The MgO barrier was formed by reactive sputtering in an argon–oxygen mixture. They used an array of microscopic probes on a wafer in which the MgO thickness increased linearly to study how the *MR* varied with barrier thickness. In contrast with the work of Yuasa *et al* [3], they found no significant variation in *MR* with MgO barrier thickness. It is perhaps not too surprising that the results from the two groups differ, since their samples are so different. As one would expect, these experimental results by the two groups generated a significant amount of subsequent work. An *MR* value of 271% was obtained [63] for the room-temperature magnetoresistance of a fully epitaxial bcc Co(001)/MgO(001)/Fe(001) magnetic tunnel junction. Some of these studies focused on structural and interface effects of MTJs with MgO barriers [64, 65]. For very small MgO thicknesses, the *MR* of MTJs with MgO barriers decreases [66]. One of the commercial interests for read head applications of MTJs with MgO barriers is to reduce the *RA* product without losing too much *MR*. In going to higher density recording, it is important to not let the *RA* product get too large. MTJs with MgO barriers have relatively favourable *RA* products, but at the highest densities it is likely that CPP GMR sensors will have to be used.

MTJ sensors have higher magnetoresistance values and base impedance than GMR sensors. Because of their higher impedance, MTJ sensors use less power than GMR sensors, but they have more Johnson noise. These devices often have an inherent noise that is much larger than the Johnson noise limit. Klaassen *et al* [67] give a more general discussion of noise in MTJ sensors pointing out that different noise mechanisms, such as shot noise, dominate at different bias voltages. Because of their high magnetoresistance, high impedance, and planar geometry, MTJ sensors have potential for being used as low cost, energy efficient,

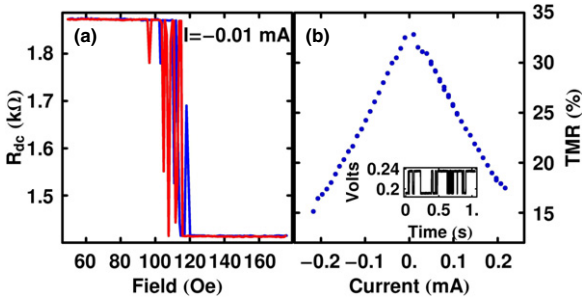

Figure 11. (a) Resistance of the MgO MTJ showing the onset of telegraph noise. (b) Tunneling *MR* as a function of current. The inset shows the fluctuation between the two states. Taken from [72].

high sensitivity magnetic sensors. A single-axis MTJ has been used to construct a two-axis magnetometer [68].

MTJs are the key element in nonvolatile random access memory (MRAM). The need for better MTJs for MRAM has motivated some of the work for MTJs with higher values of *MR*. MRAM is an alternative to the dominant three chip memory families: static random access memory (SRAM), dynamic random access memory (DRAM), and FLASH. The factors that have led researchers to find an alternative are the scaling limitations faced by each of these technologies and the desirability for system simplification that one 'universal' memory could bring. In current MRAM, the information is stored in the direction of magnetization of the soft layer of the MTJs. The direction of magnetization of the soft layer can be switched by applying either a magnetic field or a current. Downsize scalability is a problem in commercializing high capacity devices. Zhu and Zhu [69] analyze two MRAM designs, using perpendicular uniaxial anisotropy spin torque, that provide downsize scalability. One of the designs uses spin torque, first introduced by Berger [70] and Slonczewski [71]. The other design uses field switching. By having a time delay between when current is applied to the x and y write lines, a procedure called toggling, the range of parameter space for the amplitude of the x and y line write currents with allowable error rates is greatly expanded. Using spin torque switching it is possible to eliminate some write lines which, in turn, can lead to higher density MRAM. The desirable properties of MRAM are its high speed, low power consumption, long storage time, and high density. In addition, it is radiation hard. Specifically, MRAM has the high density of DRAM, the high speed of SRAM, and the non-volatility of ferroelectric random access memory (FRAM). Among the most promising new-memory candidates for near-term commercialization are field-switched MRAM, which has some potential as a universal memory, and phase-change memory, which has potential as a high density nonvolatile memory that is scalable beyond the limits of some FLASH technologies.

Because of the use of MTJs in MRAM, there is considerable interest in the bias dependence and current switching of MTJs. It is observed that the *MR* decreases if a bias voltage is applied to the MTJs. At present, there is no generally accepted explanation for this behaviour. Fuchs *et al* [72] employed the spin-torque response to study the relationship between *MR* and spin transfer when there is a bias voltage. They found that unlike the *MR*, the spin torque is independent of the bias. Their result is consistent with theoretical predictions when they included the effects of a high density of defects and lower barrier heights. They employed a very thin free layer that only had an area of 3.5×10^{-11} cm^2. Because of the small volume of the free layer, the free layer was thermally unstable at room temperature when $H - H_{\rm dip} \sim 0$. The quantity $H_{\rm dip}$ is the dipolar field. In this field range, the free layer telegraphs between the high and low resistance states. Figure 11 shows how the telegraph noise appears as a function of field and the decrease in *MR* with bias. The inset in figure 11(b) shows the fluctuations. Because of the low resistance of the junction, the current through the junctions was able to exert

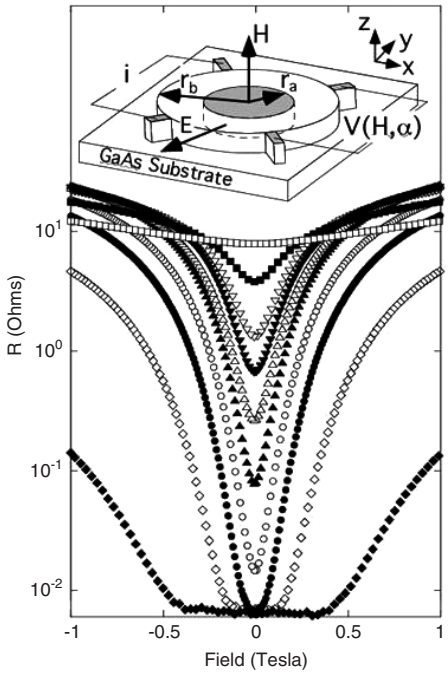

Figure 12. The room-temperature resistance as a function of field for several extraordinary magnetoresistance sensors for several values of r_a/r_b. The symbols correspond to values of $16\alpha = 0, \square$; 6, ■; 8, △; 9, ▼; 10, △; 11, ▲; 12, ○; 13, ●; 14, f; and 15, ♦. Taken from [73].

a spin-transfer torque N_{st} comparable to the magnitude of the field torque N_H. As a function of bias current, they used the telegraph noise to measure the magnetic field H where N_{st} and N_H are equal in magnitude but have opposite effects on the energy barrier for magnetization reversal. When this condition is satisfied, the lifetimes for magnetization reversal of the free layer between the states are equal.

2.5.4. Extraordinary magnetoresistance. Large values of room-temperature magnetoresistance have been obtained [73] by using narrow-gap semiconductors in a special geometry. The geometry is shown in figure 12. The sensor employs a symmetric van der Pauw disc of indium antimonide with an embedded gold inhomogeneity. The sensor does not contain any magnetic material. The magnetoresistance results from the field dependent deflection of the current around the inhomogeneity. To understand the operation of the sensor it is necessary to consider the conductivity tensor. The non-zero elements of the tensor are

$$\begin{aligned} &\sigma_{xx}(\beta) = \sigma_{yy}(\beta) = \sigma/(1+\beta^2), \qquad \sigma_{zz}(\beta) = \sigma, \\ &\sigma_{xy}(\beta) = -\sigma_{yx}(\beta) = -\sigma\beta/(1+\beta^2) \end{aligned} \tag{3}$$

where $\beta = \mu H$ and σ is the conductivity of indium antimonide. At $H = 0$, the conductivity tensor is just σ times the unity matrix. At large values of H, the off-diagonal elements dominate and the current is perpendicular to the applied field. Thus, the device has a low impedance at low fields and a high impedance at high fields. As can be seen from figure 12, the magnetoresistance is a strong function of the geometric parameter $\alpha = r_a/r_b$ where r_a and r_b are the radii of the gold and indium antimonide, respectively. The sensor's magnetoresistance is only weakly temperature dependent. Modeling results [74] indicate extraordinary magnetoresistance read heads might be useful for increasing the magnetic storage density to 1 Tbit in^{-2}. The signal to noise ratio (SNR) goes as the square root of sample volume. A disadvantage of the sensor is that it requires a significant biasing field.

2.5.5. Ballistic magnetoresistance. Ballistic magnetoresistance, a subject that has drawn considerable interest, involves a very small metallic contact between two ferromagnets. If the contact is small enough and there is no domain wall in the contact, electrons can pass ballistically between the two ferromagnets. The proposed mechanism [75, 76] for magnetoresistance involves non-adiabatic spin scattering across atomic scale magnetic domain walls trapped at the constriction. Values of magnetoresistance of several hundred per cent [77] at room temperature, or even larger [78], have been reported in electrodeposited Ni–Ni nanocontacts 10–30 nm in diameter, but others have not been able to reproduce the results [79]. Though magnetostriction plays a role, Sekiguchi *et al* [9] believe that there are phenomena that cannot be simply explained by magnetostriction. They used break junctions formed from Ni wire to investigate *MR* in the regime of conductance quantization where the conductance changes in units of e^2/h or $1/12\,900\ \Omega^{-1}$. They observed that large *MR* values of hundreds of per cent as a function of conductance tended to occur at integer values of e^2/h. Further, conductance changes of e^2/h were observed as a function of applied field.

2.6. Spin-valve transistors

Spin-valve transistors [80] are spin valves sandwiched between a pair of semiconductors, one of which is the emitter and the other the collector. The current through the device changes as a function of magnetic field. Current changes with increasing magnetic field as large as 200% have been observed, but, at present, the output currents are of the order of microamps and are too small for most sensor applications.

2.7. Giant magnetoimpedance (GMI) magnetic sensors

The impedance of amorphous wires and ribbons decreases sharply [81, 82] in fields less than 50 Oe. The effect has been called the giant magnetoimpedance (GMI) effect. The impedance is a strong function of both the magnetic field and the frequency of the drive current. For uniform, single-phase materials the origin of the effect is the impedance dependence of the skin depth, which is a function of the transverse permeability [83]. For NiFe/Cu composite wires, the magnitude of the impedance change peaks at a frequency of several MHz that depends on the annealing treatment of the wire. To use the effect requires using GHz drive currents.

2.8. Magnetostrictive magnetometers

2.8.1. Fibre-optic magnetometer. The fibre-optic magnetometer employs two glass fibres that are arranged to form a Mach–Zender interferometer. In the magnetometer, light from a laser passes through a beam splitter into the two fibres, travels along the length of the fibres, is recombined, and arrives at a photodetector at the end of each fibre. One of the fibres is either wrapped around or coated with a magnetostrictive material, a material whose dimensions depend on the direction and magnitude of its magnetization. When the magnetostrictive material is magnetized by an external field, the length of the fibre changes. Because of the length change, the light travelling through the fibre is out of phase with the light arriving from the reference fibre. The interference of the two light beams causes the light level at the photodetector to change by an amount dependent on the phase difference. Changes in path length as small as 10^{-13} m have been detected with this type of interferometer. The fibre-optic magnetometer has a sensitivity range of 10^{-2}–10^{6} nT. It can be employed to sense fields with frequencies below 60 kHz.

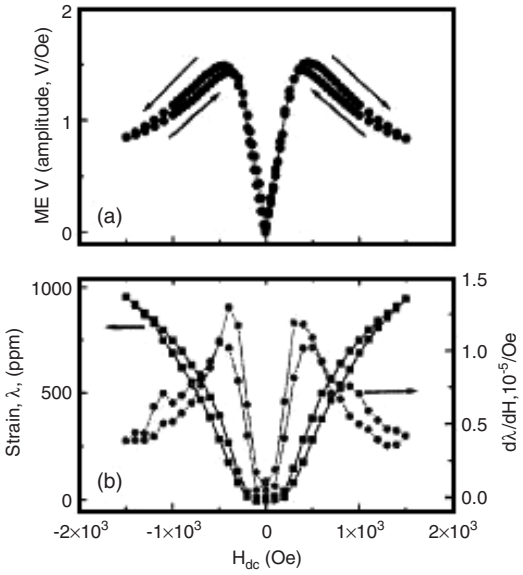

Figure 13. (a) Output voltage of ME sensor as a function of field. (b) Strain of ME sensor as a function of field. Taken from [85].

2.8.2. Magnetoelectric (ME) sensor. Another interesting method for measuring the vector components of the magnetic field is to use laminates of magnetostrictive material and a piezoelectric material. Dong *et al* [84, 85] used a three layer laminate consisting of two layers of a magnetostrictive material Terfenol-D that surround a piezoelectric, $Pb(Mg_{1/3}Nb_{2/3})O_3$–$PbTiO_3$, to fabricate a magnetoelectric sensor that can detect changes in the pT range. The length change induced in the magnetostrictive material by the magnetic field is converted into a voltage in the piezoelectric material. The symmetric geometry optimizes the elastic coupling between the layers. Figure 13(a) shows the magnetoelectric (ME) voltage as a function of the magnetic field. The strain induced as a function magnetic field is shown in figure 13(b). One sees that the ME voltage coefficient $\partial V_{\mathrm{ME}}/\partial H$ is strongly dependent on the strength of the dc field H_{dc}. Because the response at low fields is nonlinear, it is necessary to bias the device with a dc field. Initially it was necessary to use fields of order 100 or more Oe, but later work [86] shows that much lower fields are required if the Terfenol-D is replaced by metglass which saturates in a much smaller field. The piezoelectric must be poled[1] and can operate when poled in different directions [4]. The bias field can be supplied by a permanent magnet, but vibrations of the magnet will be a source of noise. The laminate had a giant magnetoelectric coefficient of $\sim$1.6 V Oe^{-1} when the device was biased in a dc field of 450 Oe. The device requires no energy to generate this voltage. The ME voltage rolls off below a frequency f_{cut}. This frequency was reduced using a multilayer composite [5] operating in the L–T mode. In the L–T mode, the layers are magnetized longitudinally and the piezoelectric material is polarized transversely. In their device, $f_{\mathrm{cut}} = 1/2\pi\tau$ where $\tau = NRC_o$ and N is the number of piezoelectric layers, R is the lesser of the laminate resistance and the input resistance of the electrometer, and C_o is the capacitance of an individual piezoelectric layer. Thus, to get τ large one must use an electrometer with a high input impedance ($>10^9$ Ω). A lock-in amplifier set with a time constant of seconds was used to obtain low frequency data. They were able to obtain a flat frequency response from $\sim 5 \times 10^{-3}$ Hz to greater than 100 Hz. They measured sensitivities of 100, 1 and 10^{-2} nT for frequencies of 10^{-2}, 1, and 10^2 Hz, respectively.

[1] Poling is inducing a residual electric polarization by applying and removing an electric field.

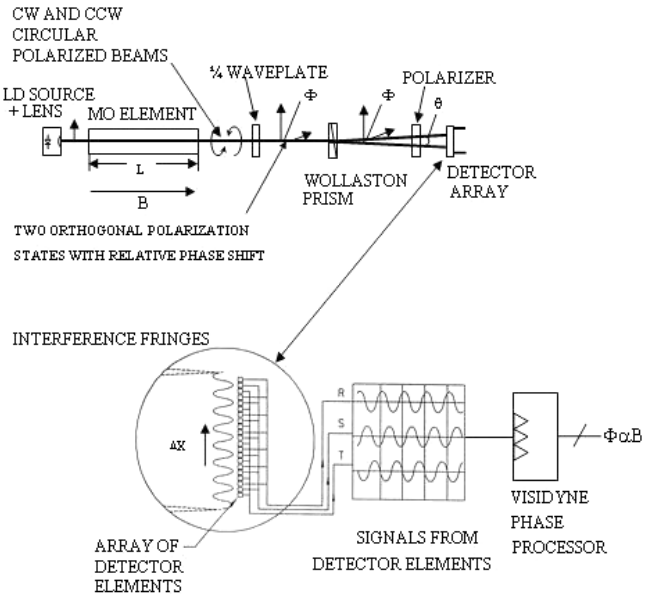

Figure 14. Operation of magneto-optic magnetometer based on the interference of two optical beams one of which passes through the magneto-optic materials YIG. Courtesy of Visidyne, Burlington, MA.

2.9. Magneto-optical sensor

The magneto-optical sensor uses the Faraday rotation of the plane of polarized light travelling through a magnetic material. The effect is largest in a few crystals when the propagation directions of the light, the crystal axis, and the applied magnetic field are all aligned. The Faraday effect results from the fact that the crystal's index of refraction is different if the electrons precess about the longitudinal magnetic field in the same or the opposite sense as the rotation of the electric field of the circularly polarized light. A figure of merit used to compare this effect between materials is the Verdet constant V, which has units of angular rotation per unit of applied field per unit of material length. Figure 14 illustrates the case of a phase difference between the two circularly polarized beams after they pass through the magnetically optic material (MO). The phase difference is given by $2BVL$, where L is the optical path length in the MO and B is the magnetic field strength. The phase difference gives rise to interference fringes in the detector array which can be measured as a ratiometric quantity. By measuring this phase shift directly as a ratiometric quantity, the resulting signal is unaffected by laser intensity noise. Using this approach, phase shifts as small as one part per million can be measured. Another useful innovation is the use of low frequency feedback coils to maintain the detector's operating point. The balance point between the two polarizations can drift significantly over a short period of time (minutes) due to slow changes in the ambient geomagnetic field. Using feedback to maintain a nearly constant polarization rotation allows significant gain to be applied to the higher frequency signal. It is possible to construct laboratory top magneto-optical magnetometers with a sensitivity of 30 pT.

A common magneto-optic material for field sensing is terbium gallium garnet, which has a Verdet constant of 0.5 min/(G cm). Along with a relatively high Verdet constant, this material can also have a permanent magnetization. Because of this unique combination of magnetic characteristics, this material has more applications in magneto-optical memories than in sensors. The unique advantage that the magneto-optical sensor has over other magnetic sensors is its very fast response time. Magneto-optical sensors with gigahertz response have been fabricated.

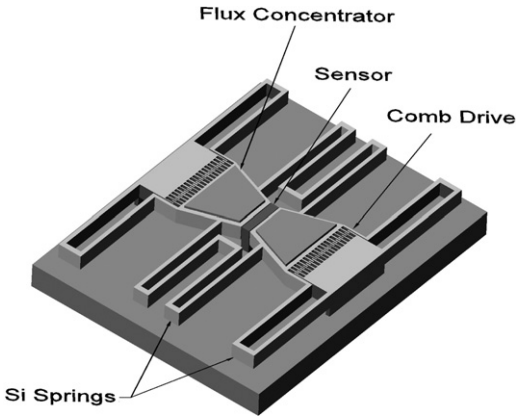

Figure 15. Picture showing the concept of the MEMS flux concentrator. Note that there is a space between the substrate and the flux concentrators on the MEMS flaps.

2.10. MEMS-based magnetometers

Many of the earliest designs of magnetic sensors utilized simple magnetic attraction to ferrous objects. The resulting motion was then measured to record or detect metal objects. A structure similar to a compass needle was the first magnetic field triggered fuze for mines. With the growth of microfabrication, i.e., MEMS (micro electro mechanical systems), the idea of using movement to sense magnetic fields has been reexamined. As we will see, MEMS technology can be applied to magnetometry in several different ways. Fabricating MEMS magnetometers is generally challenging. This is especially true if the fabrication process requires using different technologies that are not naturally compatible. For example, the use of HF, often required to perform the release step in MEMS fabrication, can damage other parts of the sensor.

Some MEMS-based magnetometers are still based on detecting the motion of a miniature bar magnet [87]. The hard magnetic material used was deposited by electrodeposition. The choice of materials for the hard magnet was limited by the need to use HF in the release step. The bar magnetic responds to the field without drawing any power. Fields as small as 200 nT have been detected optically. A similar approach was employed by DiLella *et al* [88] who also use the rotation of a MEMS structure containing a permanent magnet. In this case, the field is determined by measuring the feedback required to maintain a constant tunneling current. They achieved a resolution of 0.3 nT $(\mathrm{Hz})^{-1/2}$ at 1 Hz. The sensitivity was limited by air pressure fluctuations. An alternative approach uses a xylophone resonator [89]. In this approach, an ac current whose frequency is adjusted to be equal to the resonant frequency f_o of a MEMS beam is sent through the length of the beam. A dc field applied perpendicular to the axis of the beam will energize motion of the beam at the frequency f_o. The amplitude of the motion, that can be detected optically, is proportional to the field. A commercial MEMS magnetometer is being developed by mPhase Technologies and Lucent Bell Laboratories that measures small changes in capacitance.

MEMS technology can improve magnetic sensors by minimizing the effect of $1/f$ noise. The concept for a device that can accomplish this, the MEMS flux concentrator [6, 18], is shown in figure 15. In the device, the flux concentrators composed of a soft magnetic material, permalloy, are deposited on MEMS flaps. The flux concentrators enhance the field at the position of the magnetic sensor. Decreasing the separation between the flaps increases the enhancement. The two MEMS flaps are forced to oscillate by applying an ac voltage to the electrostatic comb drives. Because the teeth of the comb are pulled together independently of the sign of the applied voltage, the field at the sensor is modulated at twice the frequency of

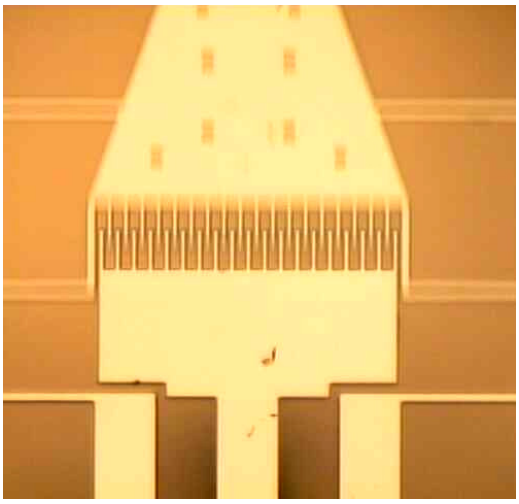

Figure 16. MEMS structure driven at its normal mode resonant frequency of 15 kHz. The portion of the picture that appears out of focus shows the portion of the structure that is oscillating with an amplitude of 12 μm.

the applied drive voltage. By tuning the frequency, one can excite the normal mode in which the distance between the flaps oscillates. The resonant frequency for the MEMS structure is designed to be about 10 kHz. The oscillation of the MEMS flaps modulates the field at the position of the sensor and, hence, shifts the operating frequency of the sensor above the frequency where $1/f$ noise dominates. Depending on the type of magnetic sensor used, this shift in operating frequency should increase the sensitivity of magnetometers at 1 Hz by one to three orders of magnitude.

The MEMS flaps are connected by a silicon spring so that there is an in-plane normal mode for the motion in which the separation between the flaps is oscillatory. Spin-valve sensors are used in the proof of concept device because spin valves are a relatively mature technology and because they have a considerable amount of $1/f$ noise. Several difficulties were encountered in fabricating the MEMS flux concentrator. Silicon on insulator (SOI) wafers were used because using these wafers decreases the number of processing steps. It was found, however, that only specially selected SOI wafers could be used. If the bonding between the device Si layer and the Si handle layer was not good enough, the HF etch was so anisotropic that it was impossible to release the MEMS structure without also etching away the supporting SiO_2 anchors between the MEMS structure and the Si handle layer. A more serious problem was the fact that the HF used in releasing the MEMS structure destroyed the spin-valve sensors. Several attempts at finding a protective layer that could be used to cover the spin valves proved unsuccessful. However, two solutions were found to this problem. Both solutions avoid exposing the spin valve to HF. The first method is to use SOI wafers in which the insulator is epoxy. The release is done in an oxygen plasma and HF is never used in the processing. Care must be exercised to avoid overheating in performing the release. In the second method, to avoid damaging the spin valve, the MEMS structure and the magnetic sensor are fabricated on different wafers. The wafers are then diced and flip chip bonding is used to complete the processing. No heating is used in the flip chip bonding. The bonding is done by compressing indium bumps. This approach has the advantage that one can test different magnetic sensors to optimize performance without having to fabricate new MEMS structures that can only be used for the test.

Figure 16 shows a picture of a MEMS flux concentrator being driven in the normal mode motion where the distance between the flaps oscillates. The motion occurs at a resonant frequency of 15 kHz. Though a 50 V drive voltage is required to obtain a 12 μm amplitude

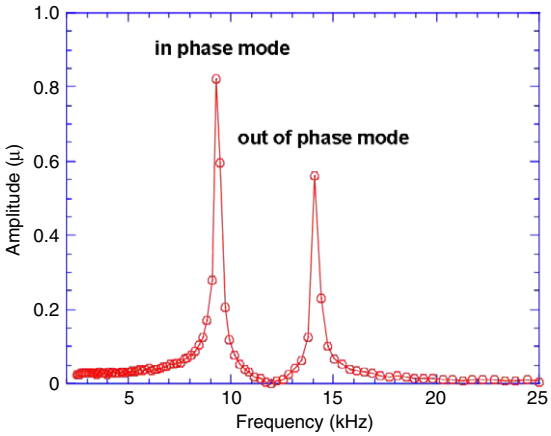

Figure 17. Amplitude of the motion of a MEMS structure showing the two low frequency normal modes.

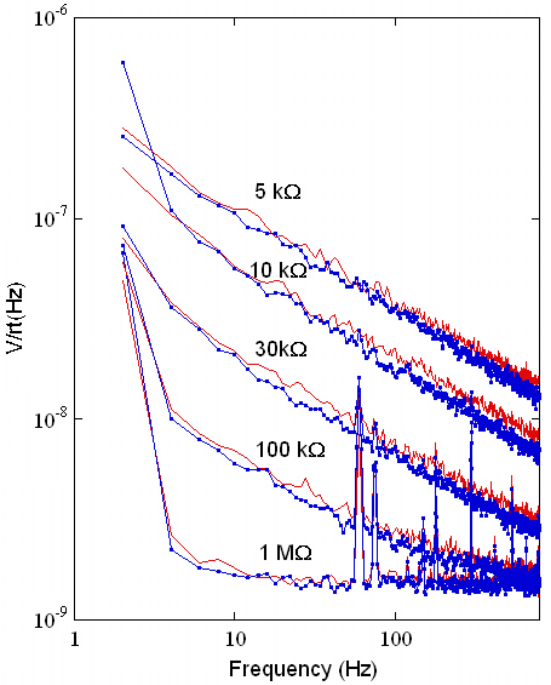

Figure 18. The noise voltage of spin valves with (dotted line) and without (solid line) flux concentrators. The curves are labelled by the value of the resistor in series with the spin valve.

for the motion, the voltage required will be reduced by at least a factor of three when the device is vacuum packaged. Figure 17 shows the amplitude of the motion of one of the devices as a function of frequency. One sees two in-plane normal modes. In the lower frequency mode, the separation between the flaps remains constant. In the higher frequency mode, the desired mode, the separation between the flaps oscillates and will modulate the magnetic field at the position of the sensor. Measurements were performed to insure that adding the flux concentrator does not increase the sensor noise. The noise with and without the flux concentrator, as a function of frequency, is shown in figure 18. One sees that there is no difference between the noise with and without the flux concentrator and, hence, within the accuracy of our measurements the flux concentrator does not increase the noise. Measurements of the noise with a magnetic field modulating the MEMS flux concentrator showed that small

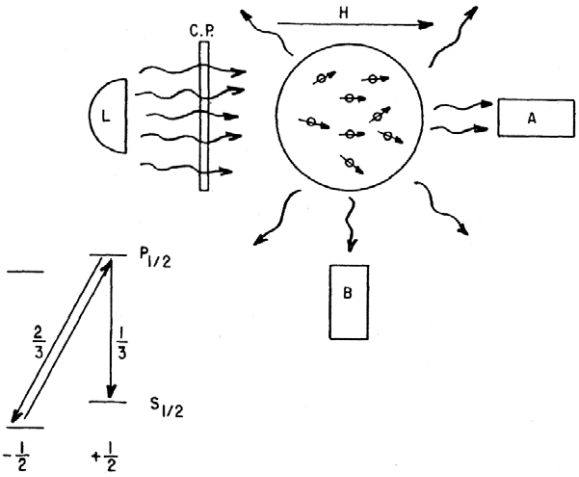

Figure 19. Illustration of the atomic energy levels and components used in a simple optical pumped magnetometer. Taken from [97].

field modulations, like those generated by the motion of the MEMS flaps, do not increase noise due to the flux concentrator.

2.10.1. Magnetoresistance of Kondo-assisted tunneling in C_{60}. An interesting effect was discovered [8] at helium temperatures in studies of the tunneling through C_{60} molecules with ferromagnetic nickel electrodes. Pasupathy *et al* used electron beam lithography and electromigration to produce fine lines with a nanoscale gap. C_{60} molecules were deposited to bridge this gap. The conductance of some of their samples with gold electrodes exhibited a zero voltage peak that is associated with the Kondo effect. This peak split when a magnetic field was applied. The ferromagnetic Ni electrodes were shaped so that their magnetizations reversed at different field values. They then measured the change in the *MR* between the parallel and antiparallel configurations of the Ni magnetizations and compared their result with the Julliere estimate, equation (2), and found reasonable agreement. What is more interesting is that when the magnetizations of the Ni electrodes are parallel the zero voltage peak is split into two peaks. The splitting disappears when the magnetizations of the two nickel electrodes are antiparallel. The splitting is too large to be associated with a Zeeman splitting and instead is due to a local exchange field. One of their samples exhibited an *MR* of 80%.

3. Total field magnetometers

Total field magnetometers have the important advantage, pointed out earlier, of insensitivity to rotational vibrations. Total field magnetometers use the fact that the splitting between some electron or nuclear spin energy levels is proportional to the magnetic field over a field range sufficient for magnetometry. Obtaining high sensitivity requires using resonances with narrow lines with long lifetimes. Such lines limit the sampling frequency. Thus, the sensitivity of these magnetometers decreases rapidly for frequencies above 10 Hz.

3.1. Optically pumped magnetometer

Optically pumped energy levels can be used both in atomic clocks and magnetometers. Figure 19 shows the energy levels and a simple version of the apparatus. Suppose an alkali metal atom with a $^2S_{1/2}$ ground state and a $^2P_{1/2}$ excited state is illuminated with circularly

polarized light. Light absorption can occur only by transitions from the ground state $-1/2$ sublevel to the $+1/2$ sublevel $^2P_{1/2}$ excited state. Atoms in the $+1/2$ sublevel $^2P_{1/2}$ excited state decay quickly into the ground state. The atoms are twice as likely to decay into the $-1/2$ ground level as the $+1/2$ ground level. Nevertheless, if there is no relaxation mechanism for atoms in the $+1/2$ ground level, then all the atoms will be 'pumped' into the $+1/2$ level. The pumping can be detected by the increased intensity of the transmitted light at A (see figure 19) or the decrease in the fluorescence measured at B due to the decrease in resonant scattering of light. One then measures the frequency of the radiation needed to induce transitions between the $+1/2$ ground state level and the $-1/2$ ground state level. This frequency can be measured by a decrease in transmitted intensity at A or an increase in fluorescence at B. It is possible to use the same apparatus with small or no modification as either an atomic clock or a magnetometer by using different energy levels. For clocks, one chooses energy levels that are insensitive to the magnetic field. For a magnetometer, one chooses energy levels that are sensitive to the magnetic field. In some cases, depending on the magnitude and direction of the magnetic field, optically pumped magnetometers can be either total field magnetometers or vector magnetometers. Optically pumped magnetometers have the advantage that they need no calibration since the spin precession frequency of alkali atoms has a known, direct relation to the magnetic field.

For application either as a clock or a magnetometer the energy levels must be narrow and, therefore, the lifetimes long. Long lifetimes are obtained by using the vapour phase, a buffer gas, and antirelaxation coatings on the cell walls. The buffer gas slows down diffusion and, thus, decreases collisions with the walls or atoms that cause spin relaxation. In cells with antirelaxation coatings, polarized alkali atoms can experience up to 10^4 collisions with the wall without depolarization. For example, intrinsic Zeeman relaxation rates of 20 Hz have been observed in 3 mm diameter glass cells containing Cs vapour in which the inner walls have been coated with paraffin [90]. In addition, high light intensities can lead to narrow line widths. Nonlinear magneto-optical rotation (NMOR) linewidths of $\sim 2\pi \times 1$ Hz have been observed [91] for atoms in paraffin-coated cells. Cold atoms prepared by laser trapping and cooling have been used for NMOR-based magnetometry to measure a field of 0.18 μG. In the experiment, $\sim 10^8$ cold ^{85}Rb atoms were trapped in a magneto-optical trap (MOT) and then released for measurement [92]. There have been suggestions for making high sensitivity optical magnetometers. For example, Scully and Fleischhauer [93] discussed how one might use an index-enhanced medium to make a magnetometer that could detect 10^{-12} G. Novikova *et al* [94] found a frequency where the different Stark shifts of the nonlinear magneto-optic effect cancel. Eliminating this source of broadening could increase the sensitivity of optical magnetometers. Pulz *et al* [95] discuss a new tandem magnetometer. Tandem magnetometers combine the fast response of a self-oscillating vapour magnetometer with the accuracy of an M_z magnetometer.

The fundamental sensitivity limit of optically pumped magnetometers [96] is due to shot noise and is given by

$$\delta B = \frac{1}{\gamma \sqrt{n T_2 V t}} \tag{4}$$

where n is the density of atoms, γ is their gyromagnetic ratio, T_2 is the transverse spin relaxation time, V is the volume of the cell, and t is the measurement time. Spin exchange often limits T_2. Experiments showed that one could eliminate spin-exchange relaxation by using a high potassium (K) pressure, He buffer gas, and a very low magnetic field [96]. By eliminating spin-exchange relaxation using a high potassium density and low magnetic fields a sensitivity of 10 fT or 10^{-5} nT Hz$^{-1/2}$ was achieved in an optically pumped K magnetometer [96].

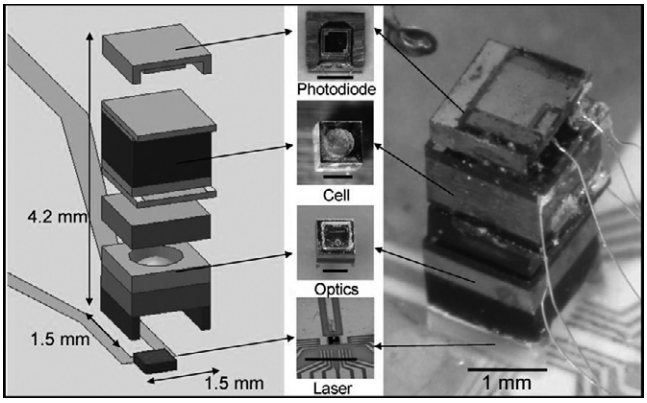

Figure 20. Picture of the chip-scale atomic magnetometer that shows the stack of elements needed to make it operate. The cell is filled with Cs and a buffer gas. Taken from [7].

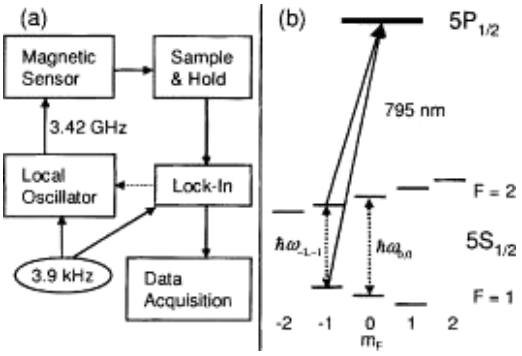

Figure 21. (a) Block diagram of chip-scale atomic magnetometer system. (b) Energy level diagram of ^{87}Rb showing the resonant first-order sidebands. Taken from [7].

Unfortunately, these long relaxation times also imply that increasing the measurement sampling rate will decrease the sensitivity.

Typical sensitivities for cesium and helium vapour sensors are 700 kHz G^{-1} and 2.8 MHz G^{-1}, respectively and these optically pumped magnetometers have a sensitivity range of 10^{-3}–10^{5} nT. One difficulty is that the signal becomes very small when the field is oriented in some directions called dead zones. This difficulty is overcome by using several sensors with different orientations for their light-pumping beams. Reducing the cell size can cause problems because it increases collisions with the cell walls that limit the spin lifetime. A problem with using He is that it tends to diffuse through the cell walls. Several reviews have been written on optically pumped magnetometers [97, 98].

At present, optically pumped magnetometers are costly, the glass cell containing the alkali gas is relatively large, about 100 cm^3, and they consume several watts of power. There are efforts to construct magnetometers that have better characteristics with respect to cost, size, and power consumption. One such effort [7] is the chip-scale magnetometer shown in figures 20 and 21. The magnetometer consists of a stack of elements that is amenable to low cost, wafer level fabrication. At one end of the stack is a vertical-cavity surface-emitting laser (VCSEL). Next in the stack is the micro-optics package that attenuates, circularly polarizes, and collimates the beam. The beam then passes through a microfabricated rubidium vapour cell that is made by anodically bonding glass to both sides of a 1 mm thick silicon wafer with a 1 mm^2 hole. The beam is detected by a p–i–n silicon photodiode. The cell is filled with ^{87}Rb and buffer gas that is a mixture of argon and neon. The cell is heated to 120 °C to maintain the necessary density of Rb atoms by two transparent indium tin oxide (ITO) heaters on each side of the cell. The power

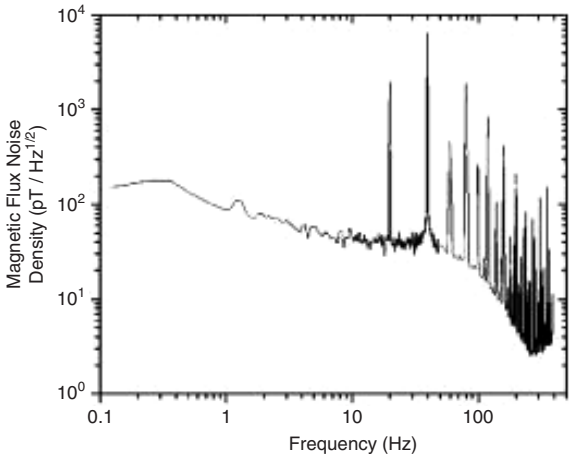

Figure 22. Power spectral density from chip-scale atomic magnetometer converted to units of magnetic field. Taken from [7].

dissipated by the heaters, 160 mW, is the largest power drain of the magnetometer. The $5S_{1/2}$ ground state hyperfine spitting between two Zeeman states was probed via coherent population trapping [99] (CPT) resonance. Using this approach eliminates the need for a microwave cavity that would increase the size of the device. The Zeeman splitting between the $F = 1$ and 2 hyperfine manifolds for small fields B is given by

$$\hbar\omega_{m_1,m_2}, = \hbar\omega_{0,0} + (m_1 + m_2)\gamma B \tag{5}$$

where $\hbar\omega_{0,0}$ is the energy difference between the magnetically insensitive states $|F = 1, m_1 = 0\rangle$ and $|F = 2, m_2 = 0\rangle$, m_1 and m_2 are the azimuthal quantum numbers for the $F = 1$ and 2 states, and γ is the gyromagnetic ratio for the atom. Note from equation (5) that the magnetometer is a scalar magnetometer. However, the magnetometer becomes a vector magnetometer if a field considerably larger than the ambient field is applied in the direction of measurement.

To use the magnetometer they tuned the VCSEL to the D1 line of ^{87}Rb at 795 nm and employed a local oscillator to amplitude modulate the VCSEL at 3.4 GHz, one-half of the hyperfine splitting of the Rb ground state. This modulation creates two first-order sidebands that are simultaneously resonant with the two hyperfine ground states to the $P_{1/2}$ excited state (see figure 21(b)). When the frequency difference of the two sidebands equals the Zeeman splitting, atoms are optically pumped into a coherent dark state and a reduction in the absorbed power is observed. The sensitivity of the magnetometer is determined by the laser amplitude noise and the shot noise from the detected photocurrent. The spectral noise power as a function of frequency is shown in figure 22. The measured sensitivity of the magnetometer is 50 pT $Hz^{-1/2}$ at 10 Hz bandwidth. Considerable work is required to make these laboratory units into stable units that can be used in the field. Though these 'chip-scale atomic magnetometers' may never reach the sensitivity of the best current optically pumped magnetometers, they are much smaller and have the potential to be much lower in cost and energy consumption.

Optical pumping of nuclear spins can be used also in magnetometry. For example, a magnetometer can be constructed using He^3. The He^3 is optically pumped, and then the precession frequency of the atomic nuclei is recorded with pickup coils. Because of the very long relaxation time of the He^3 nuclear spins, the magnetometer only requires power during the short time when the spins are excited. The sensitivity of this sensor is 10^{-3} nT and it uses less than 0.5 W.

3.2. Overhauser magnetometer

Overhauser magnetometers use an effect predicted [100, 101] by Overhauser when he was a graduate student at Berkeley in the 1950s. He predicted that in some systems you can get a factor of 1000 increase in the nuclear polarization by saturating the electron spin resonance. This increase occurs because the proton spins and electron spins interact via the hyperfine term in the Hamiltonian. The substance used in Overhauser magnetometers is a liquid containing protons and free radicals. Free radicals are molecules with unpaired electrons that have electron resonant line widths that are very narrow, about 1 Oe. The narrow line width allows one to saturate the electron resonance and hence increase the proton polarization without using much power. The magnetic field is determined by measuring the proton precession frequency which is proportional to the magnetic field. The increased proton polarization increases the signal strength. Overhauser magnetometers can achieve noise levels of 0.015 nT $Hz^{-1/2}$ at 1 Hz. Overhauser magnetometers are an order of magnitude more sensitive than proton precession magnetometers and have no dead zones.

4. Technological limitations

In this section some of the general technological limitations of magnetometer technology are discussed. One pervasive limitation is the cost and power consumption of the signal processing electronics. There is not much benefit in reducing the cost of the sensor element if the cost of the signal processing electronics dominates the cost of the magnetometer. Materials or phenomena such as the colossal magnetoresistance that have large temperature dependences cannot be used for many applications. It is also undesirable for the sensor to require a bias magnetic field. If an electromagnetic is used for the biasing, extra power is required. Using a permanent magnet for biasing will increase the noise if there are vibrations that change the field, can cause problems with field inhomogeneity, and give rise to a possible added temperature dependence. It is difficult to make sensitive measurements at low frequencies because geomagnetic noise has an approximately $1/f$ frequency dependence. Solar activity is an important source of this noise, but it is also clear that seasonal, diurnal, and geographic factors also play a role. Lightning and other broadband impulses are sources of noise. The space between the earth's surface, which is a good conductor, and the ionosphere is a resonant cavity. Lightning and other broadband impulses excite Schumann resonances [102, 103] that globally fill this resonant cavity with radiation at frequencies 7.8, 14, 20, 26, 33, 39, and 45 Hz. The amplitudes of the Schumann resonances decrease with increasing frequency. The magnitude of geomagnetic noise is of order 0.1–1 nT $Hz^{-1/2}$ at 1 Hz. Because this noise is correlated laterally over distances of hundreds of metres, one can add a reference sensor that is separated from the magnetometer by a suitable distance and subtract the signal from the reference sensor to correct for geomagnetic noise. This method permits detection of sub-pT signals in ideal situations. Because the limitations that affect stationary magnetic sensors and those on vehicles are somewhat different, they are discussed separately.

4.1. Stationary magnetometers

Stationary magnetometer magnetometers are limited by magnetic noise and often the requirement of low power consumption. In some cases, one wants the sensors system to function using battery power for weeks or months. Thus, in this case the system should only use a few mW of power. As mentioned earlier, geomagnetic noise makes it difficult to make measurements at low fields. Unfortunately, in many cases, noise sources (other than

geomagnetic noise) dominate and can be as large as several nT. Much of this background noise results from human activity.

4.2. Magnetometers on vehicles

Again one is limited by magnetic noise that includes geomagnetic noise. In this case, there is the added difficulty of magnetic noise from the vehicles and ferromagnetic debris on or under the ground. Sometimes one can use the signal from a reference sensor near the source of the magnetic vehicle noise to correct for the vehicle noise. Another problem, mentioned earlier, is rotational vibrations. There are three possible solutions to this problem. One can use total field sensors, but, unfortunately, current total field sensors are expensive. Using several sensors in a rigid gradiometer configuration will largely remove the effect of the rotational vibrations. The downside of this approach is that the signal decreases as $1/r^4$, with r being the distance away from the source, instead of the usual $1/r^3$ decrease for a dipole source. Another approach for dealing with noise from rotational vibrations is to use a frequency range where this noise is negligible or, at least, is not dominant.

5. Summary

The advances described here were motivated by the many applications of magnetic sensors. Further, magnetic sensors can be used when other sensors have unwanted signals from a changing environment. Thus, because of the many civilian and military uses of magnetic sensors it has long been desirable to improve magnetic sensors. The recent advances in magnetoresistance sensors were driven by the need for improved magnetic read heads and better memory elements in MRAM. In general, the progress described in this paper offers the possibility of magnetometers that consume less power and are also smaller, have higher sensitivity, and cost less. In some cases, such as the magnetoelectric and the MEMS magnetometers, wholly new approaches were used. The improvement in MTJ sensors using MgO barriers came about because of the improved understanding of the fundamental physics. The sensitivity of magneto-optical sensors was increased by better signal processing. The chip-scale atomic magnetometer was a result of using an approach, coherent population trapping, that avoids using a microwave cavity and the development of the ability to fabricate cells in silicon chips and fill them with the appropriate vapour. Chip-scale magnetometers may provide low cost magnetometers that avoid the problem of rotational vibrations. There is still a major need to reduce the cost of the signal processing electronics since, in many cases, the signal processing electronics is much more expensive than the sensor element.

Acknowledgments

The financial support of ONR and DARPA of Army Research Laboratory work on magnetic sensors is gratefully acknowledged. Conversations with Mike Golding and David Rall were very helpful.

References

[1] d Silva F C S *et al* 2004 *Appl. Phys. Lett.* **85** 6022
[2] Parkin S S P *et al* 2004 *Nat. Mater.* **3** 862–7
[3] Yuasa S 2004 *Nat. Mater.* **3** 868–71
[4] Dong S X *et al* 2005 *Appl. Phys. Lett.* **87** 222504

[5] Dong S *et al* 2005 *Appl. Phys. Lett.* **86** 102901
[6] Edelstein A S *et al* 2006 *J. Appl. Phys.* **99** 08B317/1–6
[7] Schwindt P D D 2004 *Appl. Phys. Lett.* **85** 6409
[8] Pasupathy A N *et al* 2004 *Science* **306** 86
[9] Sekiguchi K, Saitoh E and Miyajima H 2005 *IEEE Trans. Magn.* **41** 2565
[10] Gallagher W J 2005 Recent advances in MRAM technology *IEEE Int. Symp. on VLSI Technology* p 72
[11] Lenz J E 1990 *Proc. IEEE* **78** 973
[12] Mahdi A E, Panina L and Mapps D 2003 *Sensors Actuators* A **105** 271
[13] Daughton J M *et al* 1999 *J. Phys. D: Appl. Phys.* **32** R169
[14] Lenz J and Edelstein A S 2006 *IEEE Sensors J.* **6** 631–49
[15] Campbell W H 1997 *Introduction to Geomagnetic Fields* (Cambridge: Cambridge University Press)
[16] Nor A F M *et al* 2000 *Sensors Actuators* A **81** 67
[17] v d Veerdonk R J M *et al* 1997 *J. Appl. Phys.* **82** 6152
[18] Edelstein A S and Fischer G A 2002 *J. Appl. Phys.* **91** 7795–7
[19] Ripka P 2003 *Sensors Actuators* A **106** 8
[20] Pizzella V *et al* 2001 *Supercond. Sci. Technol.* **14** R79
[21] Cantor R 2001 *Supercond. Cryoelectron.* **13** 37
[22] Deaver B S and Fairbank W M 1961 *Phys. Rev. Lett.* **7** 43
[23] Doll R and Näbauer M 1961 *Phys. Rev. Lett.* **7** 51
[24] Jenks W G, Sadeghi S S H and Wikswo J P Jr 1997 *J. Phys. D: Appl. Phys.* **30** 293
[25] Bednorz J G and Müller K A 1986 *Z. Phys.* B **64** 189
[26] Wu M K *et al* 1987 *Phys. Rev. Lett.* **58** 908
[27] Richards P L 2004 *J. Supercond.* **17** 545
[28] Meyer H-G *et al* 2005 *Phys. Status Solidi* c **2** 1504
[29] Wakai R 2004 *AIP Conf. Proc.* **724** 14
[30] Berggren K K 2004 *Proc. IEEE* **92** 1630
[31] Castellano M G *et al* 2005 *IEEE Trans. Appl. Supercond.* **15** 849
[32] Reich T, Ortlepp T and Uhlmann F H 2005 *IEEE Trans. Appl. Supercond.* **15** 304
[33] Meissner W and Ochsenfeld R 1933 *Naturwissenschaften* **21** 787
[34] Pannetier M *et al* 2004 *Science* **304** 1648
[35] Popovic R S 2004 *Hall Effect Devices* 2nd edn (Bristol: Institute of Physics Publishing)
[36] Tumanski S 2001 *Thin Film Magnetoresistive Sensors* (Bristol: Institute of Physics Publishing)
[37] Mapps D J 1997 *Sensors Actuators* A **59** 9
[38] Stutzke N A *et al* 2005 *J. Appl. Phys.* **97** 10Q107
[39] Jiang L *et al* 2004 *Phys. Rev.* B **69** 054407
[40] McGuire T R and Potter R I 1975 *IEEE Trans. Magn.* **11** 1018
[41] Lee W Y, Toney M F and Mauri D 2000 *IEEE Trans. Magn.* **36** 381
[42] Baibich M N *et al* 1988 *Phys. Rev. Lett.* **61** 2472–5
[43] Binasch G *et al* 1989 *Phys. Rev.* B **39** 4828–30
[44] Freitas P P *et al* 2000 *Sensors Actuators* A **81** 2
[45] Ehrlich A C 1993 *Phys. Rev. Lett.* **71** 2300
[46] Ehrlich A C and Gillespie D J 1993 *J. Appl. Phys.* **73** 5536
[47] Carey M J *et al* 2002 *Appl. Phys. Lett.* **81** 1044
[48] Ounadjela K *et al* 1996 *J. Magn. Magn. Mater.* **156** 267
[49] Leal J L and Kryder M H 1996 *IEEE Trans Magn.* **32** 4642
[50] Martin J I *et al* 2003 *J. Magn. Magn. Mater.* **256** 449
[51] Gijs M A M, Lenczowski S K J and Giesbers J B 1993 *Phys. Rev. Lett.* **70** 3343
[52] Moodera J S *et al* 1995 *Phys. Rev. Lett.* **74** 3273
[53] Tsymbal E Y, Mryasov O N and LeClair P R 2003 *J. Phys.: Condens. Matter* **15** R109
[54] Julliere M 1975 *Phys. Lett.* A **54** 225
[55] Sun J Z *et al* 1998 *Appl. Phys. Lett.* **73** 1008
[56] Tondra M *et al* 2000 *J. Appl. Phys.* **87** 4679
[57] Lacour D *et al* 2002 *J. Appl. Phys.* **91** 4655
[58] Montaigne F *et al* 2000 *Appl. Phys. Lett.* **76** 3286
[59] Edelstein A S p, The impedance of $Al/Al_2O_3/La$ superconducting tunnel junctions decreased by a factor of 10 overnight when stored at room temperature because the La removes oxygen atoms from the Al oxide to form the more stable La oxide. (Early work by the author)
[60] Wang D *et al* 2004 *IEEE Trans. Magn.* **40** 2269

[61] Butler W H *et al* 2001 *Phys. Rev.* B **63** 054416
[62] Mathon J and Umerski A 2001 *Phys. Rev.* B **63** 220403
[63] Yuasa S *et al* 2005 *Appl. Phys. Lett.* **87** 222508
[64] Mizuguchi M *et al* 2006 *Appl. Phys. Lett.* **88** 251901
[65] Eames M E and Inkson J C 2006 *Appl. Phys. Lett.* **88** 252511
[66] Butler J 2006 private communication
[67] Klaassen K B, Peppen J C L v and Xing X 2003 *J. Appl. Phys.* **93** 8573
[68] Kammerer J-B *et al* 2004 *IEEE Sensors J.* **4** 313
[69] Zhu X and Zhu J-G 2006 *IEEE Trans. Magn.* **42** 2739
[70] Berger L 1996 *Phys. Rev.* B **54** 9353
[71] Slonczewski J C 1996 *J. Magn. Magn. Mater.* **159** L1–7
[72] Fuchs G D *et al* 2006 *Phys. Rev. Lett.* **96** 186603
[73] Solin S A *et al* 2000 *Science* **289** 1530
[74] Moussa J *et al* 2003 *J. Appl. Phys.* **94** 1110
[75] Tatara G *et al* 1999 *Phys. Rev. Lett.* **83** 2030
[76] Dartora C A and Cabrera G G 2005 *Phys. Rev.* B **72** 064456
[77] Garcia N *et al* 2001 *Appl. Phys. Lett.* **79** 4550
[78] Chopra H D and Hua S Z 2002 *Phys. Rev.* B **66** 020403
[79] Egelhoff W F *et al* 2004 *J. Appl. Phys.* **95** 7554
[80] Erve O M J v t 2002 *Appl. Phys. Lett.* **80** 3787
[81] Beach R S and Berkowitz A E 1994 *Appl. Phys. Lett.* **64** 3652
[82] Li X P *et al* 2003 *J. Appl. Phys.* **94** 7626
[83] Xiao S *et al* 2000 *Phys. Rev.* B **61** 5734
[84] Dong S, Le J-F and Viehland D 2003 *Appl. Phys. Lett.* **83** 2265
[85] Dong S *et al* 2005 *Appl. Phys. Lett.* **87** 62502
[86] Viehland 2005 private communication
[87] Yang H H *et al* 2002 *Sensors Actuators* A **97/98** 88
[88] DiLella D *et al* 2000 *Sensors Actuators* A **86** 8
[89] Givens R B *et al* 1996 *Appl. Phys. Lett.* **69** 2755
[90] Balabas M V *et al* 2006 *J. Opt. Soc. Am.* B **23** 1001
[91] Budker D *et al* 1998 *Phys. Rev. Lett.* **81** 5788
[92] Isayama T *et al* 1999 *Phys. Rev.* A **59** 4836
[93] Scully M O and Fleischhauer M 1992 *Phys. Rev. Lett.* **69** 1360
[94] Novikova I *et al* 2001 *Phys. Rev.* A **63** 063802
[95] Pulz E, Jäckel K-H and Linthe H-J 1999 *Meas. Sci. Technol.* **10** 1025
[96] Allred J C *et al* 2002 *Phys. Rev. Lett.* **89** 130801
[97] Happer W 1972 *Rev. Mod. Phys.* **44** 169
[98] Budker D *et al* 2002 *Rev. Mod. Phys.* **74** 1153
[99] Stahler M *et al* 2001 *Europhys. Lett.* **54** 323
[100] Overhauser A W 1953 *Phys. Rev.* **91** 476
[101] Overhauser A W 1953 *Phys. Rev.* **92** 411
[102] Schumann W O 1952 *Z. Naturf.* a **7** 149
[103] Bliokh P V, Nikolaenko A P and Filippov Y F 1980 *Schumann Resonances in the Earth-Ionosphere Cavity* (Stevenage: Peter Perigrinus)